Barotropic and baroclinic tides in Panay Strait, Philippines

Charina Lyn Amedo-Repollo [a],[*], Xavier Flores-Vidal [b], Cedric Chavanne [c],
Cesar L. Villanoy [a], Pierre Flament [d]

[a] *Marine Science Institute, University of the Philippines, Diliman, Quezon City, 1101, Philippines*
[b] *Universitad Autonoma de Baja California, Ensenada, Mexico*
[c] *Institut des Sciences de la Mer de Rimouski, Université du Québec à Rimouski, Rimouski, Canada*
[d] *University of Hawaii at Manoa, Honolulu, Hawai'i, USA*

ARTICLE INFO

ABSTRACT

The Panay Strait constitutes a bathymetrically complex system with intense tidal currents. The four major tidal constituents in the total energy spectra inferred from sea level and current profiles are K_1, O_1, M_2, and S_2. Spatially, O_1 and M_2 dominate over K_1 and S_2, respectively. The diurnal tide accounts for highest amplitude variability over the shallow shelf while semi-diurnal tides over the deeper channel of the strait. Rotary spectra of surface currents shows inertial frequency peaks and exhibit an unusually broad peak in both the clockwise (CW) and counterclockwise (CCW) rotating components, indicating frequency shift by the vorticity of sub-inertial currents prevalent in the region. Vertically, variance of the horizontal velocity explained by the major tidal constituents peaks in two distinct depth bands; the upper layer centered at 110 m (11% variance) dominated by semi-diurnal tide (M_2) and the lower layer at 470 m (26% variance) dominated by diurnal tides (O_1). Semi-diurnal tidal current ellipses (M_2 and S_2) exhibit a dominance of CW motions at near-surface depth (110 m), indicative of downward energy propagation and implying a surface energy source. These features from Acoustic Doppler Current Profiler (ADCP) deployed close to the sill is consistent with the dominant semi-diurnal tide (M_2) over the channel of the strait from the High Frequency Doppler Radar (HFDR). Comparison of incoherent to coherent tidal energy shows K_1 dominated the incoherent tidal band. Spatially, incoherent energy is dominant over the channel particularly near the sill and the constricted part of the strait. The incoherent portion of the tide is presumably attributable to the surface expression of the internal tide which seems to be generated near the sill and then topographically steered west over the edge of the shallow shelf where incoherent energy is dominant.

© 2021 Elsevier B.V. All rights reserved.

1. Introduction

Tidal currents constitute the most ubiquitous signal in the coastal ocean. They can be difficult to interpret as they vary at multiple bathymetric scales. The Philippine Archipelago bounded by the Pacific Ocean on the east and South China Sea (SCS) on the west, consists of a complex array of islands, embayments and seas connected by multitude of straits and sills. The barotropic (depth-independent) tidal components are significant in the region with strikingly different geographical structures, dominated by semi-diurnal tides in the Pacific and diurnal tides in the SCS. Within the Philippines, strong barotropic tidal flows vary strongly through many of the passages and around islands separating seas.

Tidal currents flowing over bathymetry in a stratified ocean give rise to baroclinic internal tides. In the interior Philippine seas, the signatures of active internal waves in Sulu Sea (SS) have

been observed since 1973 via visible-wavelength imagery (Apel et al., 1985). A comprehensive study using extensive dataset with theoretical and numerical analyses presented a large-amplitude internal wave generated by intense tidal flow over a sharp bathymetric feature. Apel et al. (1985) gave unprecedented information on the spatial and temporal characteristics in good agreement with surface and subsurface observations from satellite data, suggesting SS as an ideal natural laboratory to study internal wave. The SS then became a research focus for internal wave. Previous studies based on in-situ field measurements, surface signatures from remote sensing observations, and modeling work (Apel et al., 1985; Liu et al., 1985; Giese et al., 1998; Zeng and Alpers, 2004) collectively revealed a wealth of information associated with the generation sites, physical characteristics, temporal and spatial distribution of internal waves in the SS. In recent years, the Philippine Seas including the SS have received attention due to their critical role in thermohaline stratification, ocean circulation, biogeochemical fields, and its
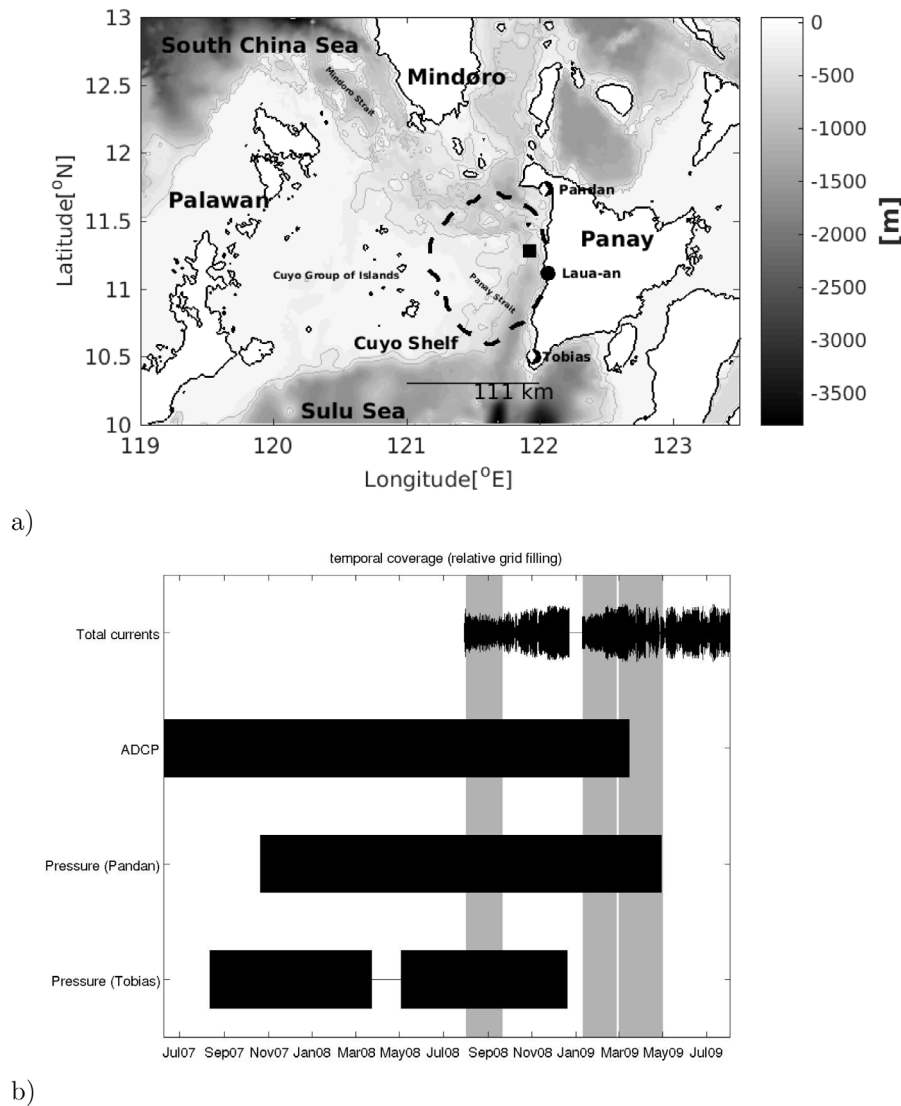
---

a)

b)

Fig. 1. (a) Bathymetry of study area and the limits of 75% HFDR data coverage indicated by thick broken line. The 200 m, 500 m, and 1000 m isobaths are shown with increasingly darker shadings. Locations of observations are marked: HFDR by circles, shallow pressure gauges by white diamonds, and ADCP by square. (b) Temporal coverage of the instruments. The thickness corresponds to the percentage of grid points with data.

influence on both the climate and the marine ecosystem (Gordon and Villanoy, 2011; Hurlburt et al., 2011; Lermusiaux et al., 2011). Surface and subsurface physical processes and impacts of internal waves were studied in this area using satellite data, field observations and modeling supported by the U.S. Office of Naval Research (ONR) Philippine Straits Dynamics Experiment (PhilEx) (Girton et al., 2011; Jackson et al., 2011, 2012; Tessler et al., 2012). Moreover, vigorous baroclinic tidal mixing through the strong tide-bathymetry interactions generated persistent up-welling and front isolated over the Sulu Ridge detected from suite of satellite measurements and confirmed by historical cruise observations (Jing et al., 2012). The upwelling was associated with pronounced Sea Surface Temperature (SST) cooling and phytoplankton bloom, 5–15 times greater than the adjacent SS and Celebes Sea. Interestingly, a recent study by Storlazzi et al. (2020) presented a first global maps where internal tides can provide thermal refugia that will buffer some coral reefs from future global warming, an information that may be incorporated into the decision-making process for designating marine protected area for coral reef protection and preservation.

Recent study by Zhang et al. (2020), revealed internal tides sources in SS were located at the narrow straits, between small islands or with an underwater ridge. Further analysis showed that multiple generation sites may exist in the same strait. Due to intense interaction between strong tidal currents and a local sill, sea water flowing over the strait will generate internal wave propagating in different directions. Internal wave can be generated by the tide-bathymetry interactions or by the evolution of internal tide from remote sources. Internal wave was also observed to cross isobaths in the eastern SS implying that these internal waves are not locally generated.

Aside from the well-known solitary wave occurrences in the SS (Apel et al., 1985; Hurlburt et al., 2011; Tessler et al., 2010) and the Sulu Archipelago (Jackson et al., 2011), concentrations of nonlinear internal wave activity on the shelf region (Cuyo Shelf) at the northeastern end of the SS between Palawan and Panay islands was observed in synthetic aperture radar (SAR) and optical sunglint satellite imagery (Jackson et al., 2011). These waves dissipate over the shallower shelf region after 2.5days of traveling
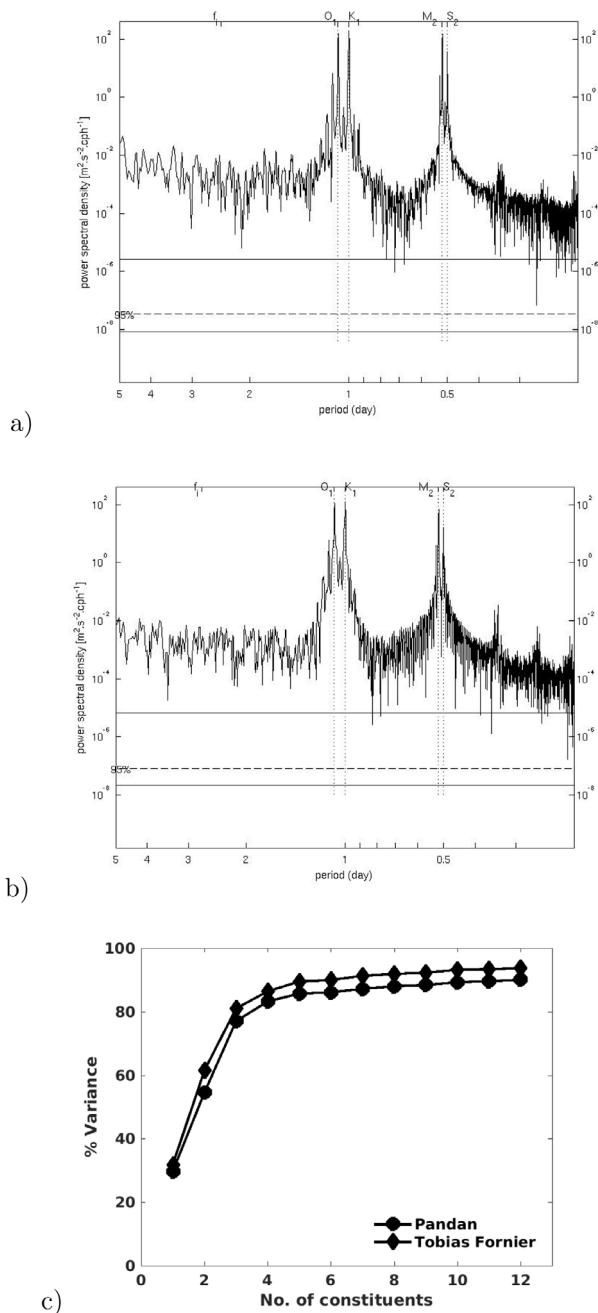
Fig. 2. Power spectral density of the time series overlap of (a) Pandan and (b) Tobias Fornier SPG, and their (c) increment variance (%) of major tidal constituents. The first 4 marked dots indicate the variance of (1) K_1, (2) K_1 and O_1, (3) K_1, O_1, and M_2, (4) K_1, O_1, M_2, and S_2.

from several locations in the Sulu Archipelago (Jackson et al., 2011). Simulations of tides in the Philippine seas by 1/12° Hybrid Coordinate Ocean Model (HYCOM) also note the strong sea surface height signature of internal tides in Mindoro Strait (Hurlburt et al., 2011). Internal wave measurements from two McLane Labs moored profilers (MMP) at either end of Mindoro–Panay Straits illustrate some similarities and dramatic contrasts over fairly short distances within archipelagic bathymetry. There are more energies to both the diurnal and semidiurnal frequency band in Mindoro Strait to the SCS while at lower (sub-inertial) frequencies with larger isopycnal displacement at depth, south of Panay Strait entering into the SS (Chinn et al., 2012).

The Panay Strait, located northwest of SS serves as the major path way of water from the SCS via the Mindoro Strait (Fig. 1a). A small basin (1300 m deep) known as the Semirara Sea separates the Panay Strait from the Mindoro Strait on the northwest and from Tablas Strait on the northeast. A sill of 578 m depth forms the shallowest point within the strait. Defining the 100 m isobath as the outer edge of the shelf, Panay Strait is bordered by the wider Cuyo shelf on the west and the very narrow Panay shelf on the east. Over the Cuyo shelf lies the low lying Cuyo Group of Islands and extensive reefs. The Panay Strait thus constitutes a topographically complex system of small low-lying islands, seamounts, shelves, sills, and a deep basin that may be a locale of intense tidal currents.

The flow within the strait is modulated by a range of processes such as tidal variations, seasonal reversal of the monsoon, sea level variations between SCS and the Pacific Ocean, interannual variations such as El Niño–Southern Oscillation (ENSO), and episodic occurrence of monsoon surges and tropical cyclones (White et al., 2003; McClean et al., 2005; Pullen et al., 2008; Han et al., 2009; May et al., 2011).

This study is one of the component of the PhilEx program with a goal of exploring the oceanography and dynamics in the narrow straits and deep basins of the Philippines using integrated insitu and remote observational methods with global and regional model components (Gordon and Villanoy, 2011). An intensive observations of Panay Strait were carried out to qualitatively and quantitatively describe the mesoscale spatial structure and temporal variability of the surface current within the strait. Three short-wave ocean current-mapping radars were deployed along the west coast of Panay Island to measure surface circulation from July 2008 to August 2009 (Fig. 1a). Further information regarding the installation, calibration and other technical details of the High Frequency Doppler Radar (HFDR) network along Panay coastline were detailed by Amedo-Repollo et al. (2019). The HFDR data helped understand the complex circulation pattern of Panay Strait.

Subject to pronounced Asian monsoon reversal, Amedo-Repollo et al. (2019) found the distinct seasonal cycle of surface circulation with the generation of a cyclonic eddy (Panay Eddy) during the northeast (NE) monsoon, reinforcing the steady Panay Coastal (PC) jet as its eastern limb. Southwest (SW) monsoon period in contrast, is characterized by a relatively weak northward PC jet, with significant weakening and modification over the shallow Cuyo Shelf. The most detailed mechanism of eddy generation and evolution was provided due to Ekman pumping without a strong oceanic flow passing the island.

For this paper, research is primarily directed towards determining the spatial structure of the barotropic and baroclinic tide in Panay Strait using HFDR-derived high frequency (hourly data) and high-resolution (5 km) datasets which have not been observed previously in an archipelagic setting like Philippines or elsewhere. Localized measurements will explore tidal interaction with the complex bathymetry that will help in the future numerical modeling and understanding tides due to prevalent regional bathymetric features.

2. Methods

For the description of tidal sea level and current oscillations, data from HFDR measurements, one moored ADCP and two shallow pressure gauges (SPG) were used. Their record lengths vary from 368 to 646 days (Fig. 1b) with about 142 days of overlap.

Failures in HFDR occurred at sites due to electrical power loss primarily because of burned power cables and generator failures during black-outs. In times when data are lost from one site, two sites were used to calculate vector currents. During the
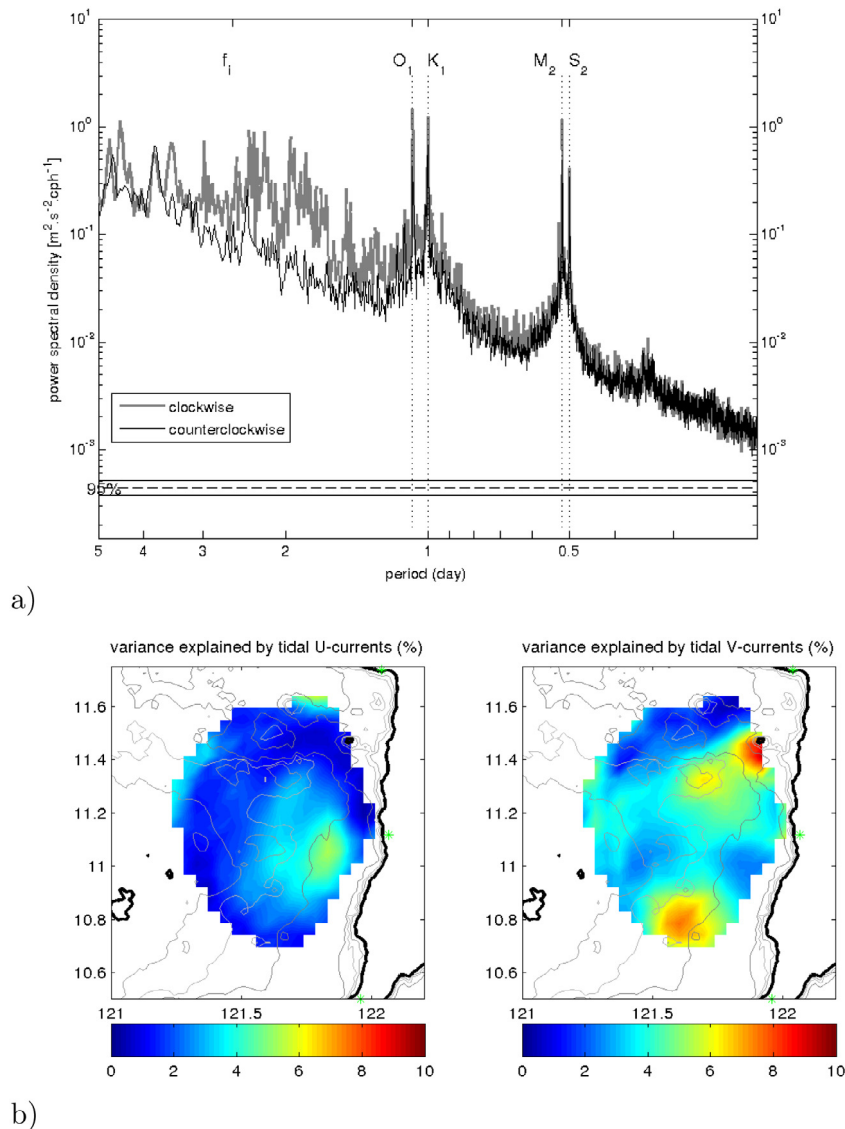
Fig. 3. (a) Rotary power spectra of HFDR data over 212 grid points with more than 75% temporal coverage. Major tidal constituents and inertial frequency, f_i are indicated on the top x-axis, indicated by vertical dotted lines. (b) Variance explained by 4 major tidal constituents (K_1, O_1, M_2, and S_2) of (left) zonal and (right) meridional surface current components.

deployment period, the largest data loss was during the bistatic calibration performed from December 22, 2008 to January 9, 2009. Moored instruments were deployed and retrieved at different times, and overlaps of uninterrupted coverage were selected for analysis.

The HFDR current vectors underwent minor quality control prior to the analysis. Missing data segments were subject to temporal interpolation (Chavanne et al., 2007) in which a constant linear trend and sinusoids at M_2, K_1 and inertial frequencies were least squares fitted to the observations available in a 3-day window centered on each missing data segment shorter than 36 h. The fit was performed only if more than 36 observations were available. This interpolation was carried out on hourly vector currents.

In conjunction with the HFDR, an ADCP mooring was deployed as part of the Exploratory Cruise on the R/V Melville in June 2007 to provide aspects of the full three-dimensional circulation in Panay Strait. An upward-looking RDI Teledyne Long Ranger 75-kHz, bottom mounted ADCP (11.2790 °N, 121.9244 °E) was located inside the region covered by HFDR, 2.5 km downstream from the narrowest constriction at Panay Sill of 578 m water

depth. The passage width is 36 km determined between the 100 m isobaths on either side of the mooring as surveyed by multi-beam echosounder. The ADCP included pressure and temperature sensors. Sampling rates were set to resolve the tides, and were 30 min for the ADCP and 15 min for the temperature sensors. The mooring was recovered in March 2009.

The ADCP returned 100% of the velocity time series. However, due to surface reflection contamination, the bottom-mounted ADCP was unable to resolve the near surface velocity (upper 50 m). Pressure time series were used to correct for mooring blowover. The velocity data were then linearly interpolated onto a 10 m depth grid and a common time base of 1 h.

As part of the PhilEx program, an array of shallow pressure gauges was deployed at approximately 5–10 m depth along Panay Strait (Pandan and Tobias Fornier, Antique). The location, deployment period and length of observation of the pressure gauges are provided in Figs. 1a and 1b. Absolute pressure is measured every ten seconds by a Paroscientific quartz pressure sensor with an accuracy of 0.3 mb (−1% of the signal). The data were averaged into hourly bins and were used to examine possible influences of sea level to the tidal variations in Panay Strait.
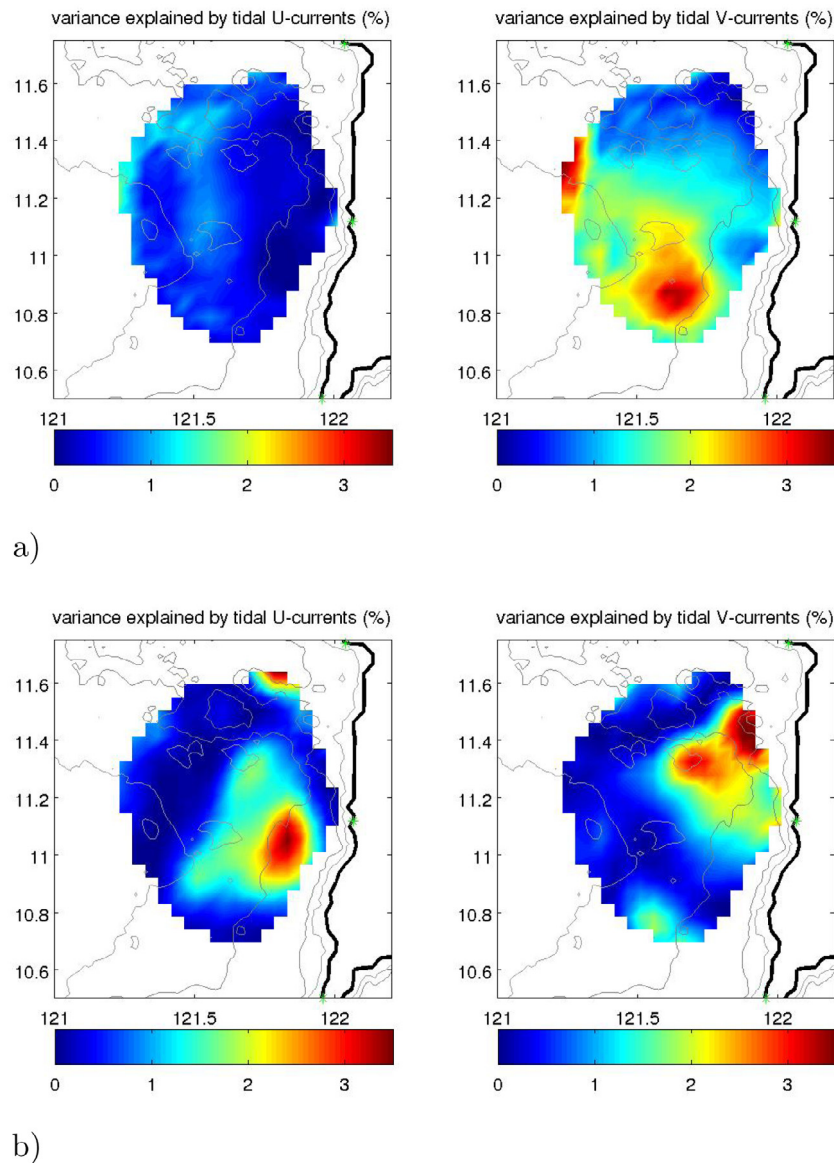
Fig. 4. Variance explained by (a) diurnal and (b) semidiurnal tidal constituents of (left) zonal and (right) meridional surface current components.

Spectral analysis is useful to partition the variance of a time series as a function of frequency (Emery and Thomson, 2004). The present study utilizes power spectrum of the sea level and rotary spectral analysis (Gonella, 1972) of the HFDR-derived surface current and current profiles from the moored ADCP. These provide estimates of power (energy density) distributed over a range of given frequency bins (Press et al., 1996). Spectral estimates were spatially-averaged for surface currents and vertically-averaged for the ADCP current profiles. The sea level spectra were further assessed to extract the tidally-driven current from the time-series data.

HFDR and ADCP current components (zonal and meridional) and sea level were harmonically analyzed using the T-Tide Matlab package (Pawlowicz et al., 2002) over the deployment period of each instrument. Four significant tidal constituents (K_1, O_1, M_2, and S_2) inferred from sea level were least square fitted to the hourly observations, along with a constant and a linear trend. The 95% confidence intervals were computed by a bootstrap method.

Maps of tidal current ellipses, major axis amplitudes and phases will be use to characterize the surface tidal currents.

The relative contribution of the tidal currents to the mean kinetic energy (KE) was estimated by the ratio:

$$R_{tmke} = \frac{\overline{u_p^2}(x,y) + \overline{v_p^2}(x,y)}{\overline{u^2}(x,y) + \overline{v^2}(x,y)} \tag{1}$$

where u and v are observed zonal and meridional current velocities, respectively and the overbar denotes a time mean of over a year record and, x and y denotes the conventional Cartesian coordinates.

Similarly, the contribution of the tidal currents to the mean eddy kinetic energy (EKE) was estimated by

$$R_{teke} = \frac{\overline{u_p^2}(x,y) + \overline{v_p^2}(x,y)}{\overline{u'^2}(x,y) + \overline{v'^2}(x,y)} \tag{2}$$

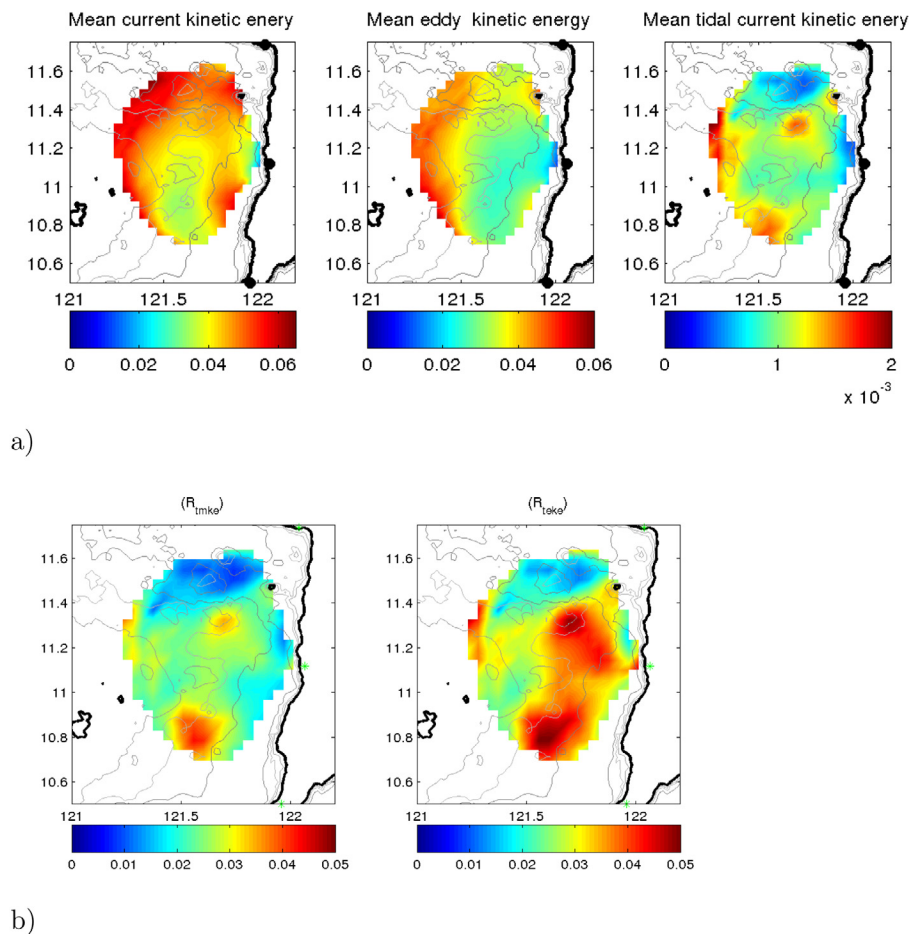where the primed quantities denote deviations from the time mean over a year.

a)

b)

Fig. 5. (a) (left) Mean kinetic energy (KE), (middle) eddy kinetic energy (EKE) and (right) tidal kinetic energy (KE). (b) Contribution of tidal currents to the (left) mean kinetic energy, R_{tmke} and the (right) eddy kinetic energy, R_{teke}.

3. Results and discussions

3.1. Tidal components inferred from sea level

Phase-locked tidal sea level explains 95.1% and 96.9% of the total sea level variance over a year (425 days) from hourly records from Pandan and Tobias Fornier, respectively. The frequency spectra of sea level variations shows energy peaks at four major constituents (K_1, O_1, M_2, and S_2) (Fig. 2a and b).

The contribution of major constituents to the total energy spectra of sea level is shown in Fig. 2c. An increase in the variance is largely attributed to K_1, O_1, M_2, and S_2, respectively. These four major constituents will therefore be use to extract tides for analysis.

3.2. Horizontal structure of the tidal components inferred from HFDR

The most energetic surface current variations for periods shorter than 5days are inertial and tidal currents. The spectral properties of surface currents within the radar domain shows diurnal peaks centered on K_1 and O_1, semi-diurnal on M_2 and S_2, and inertial frequency on f_i with period of 62 h (2.59 days) at $11.1°N$ (Fig. 3a). The O_1, K_1, M_2 and a much weaker S_2 are the most significant with minor contributions from other constituents. Higher harmonics of diurnal and semi-diurnal constituents also display significant peaks.

The rotary spectra decomposes a vector time series into CW and CCW rotating components by frequency. At near-inertial periods, the CW predominates in the northern hemisphere due to the action of the Coriolis force to the right of the velocity vector. This is evident in the spectrum where inertial frequencies have more energy in the CW rotating band as expected and are unusually broad (maximum 1.46 m^2 s^{-2} cph^{-1}), possibly frequency-shifted due to vorticity of sub-inertial currents (Amedo-Repollo et al., 2019) and the forcing by wind, both prevalent during NE monsoon (Pullen et al., 2008). For diurnal and semi-diurnal frequency bands, CW motions are also more energetic than the CCW components by 1.47 m^2 s^{-2} cph^{-1} and 1.18 m^2 s^{-2} cph^{-1}, respectively.

Variance explained by the four major tidal constituents constitute 5.7% and 9.4% of the total variance of zonal and meridional current components over the 1-year record, respectively (Fig. 3b). The highest variance for the zonal current component is over the deep channel further south of the sill and for the meridional component on the north of the sill near a sharp bend in bathymetry where the island of Batbatan is located. The semidiurnal tide contributed much to the highest variance over the deep channel while the diurnal tide over the shallow shelf (Fig. 4a and b).

The mean KE, EKE and tidal KE of the surface current are shown in Fig. 5a. The mean KE is relatively similar to EKE in terms of magnitude, though EKE tends to be greatest where the mean circulation is strongest west of the radar domain, over the shelf but low on the east along the coast. This implies that the seasonal Panay Eddy derived more of its energy from the seasonal return flow as a consequence to the positive Ekman pumping generated over this region during NEM regime and less energy from the persistent PC jet as the eastern limb of the Panay Eddy (Amedo-Repollo et al., 2019). In comparison, the mean tidal KE is an order of magnitude less than both the mean KE and mean EKE.
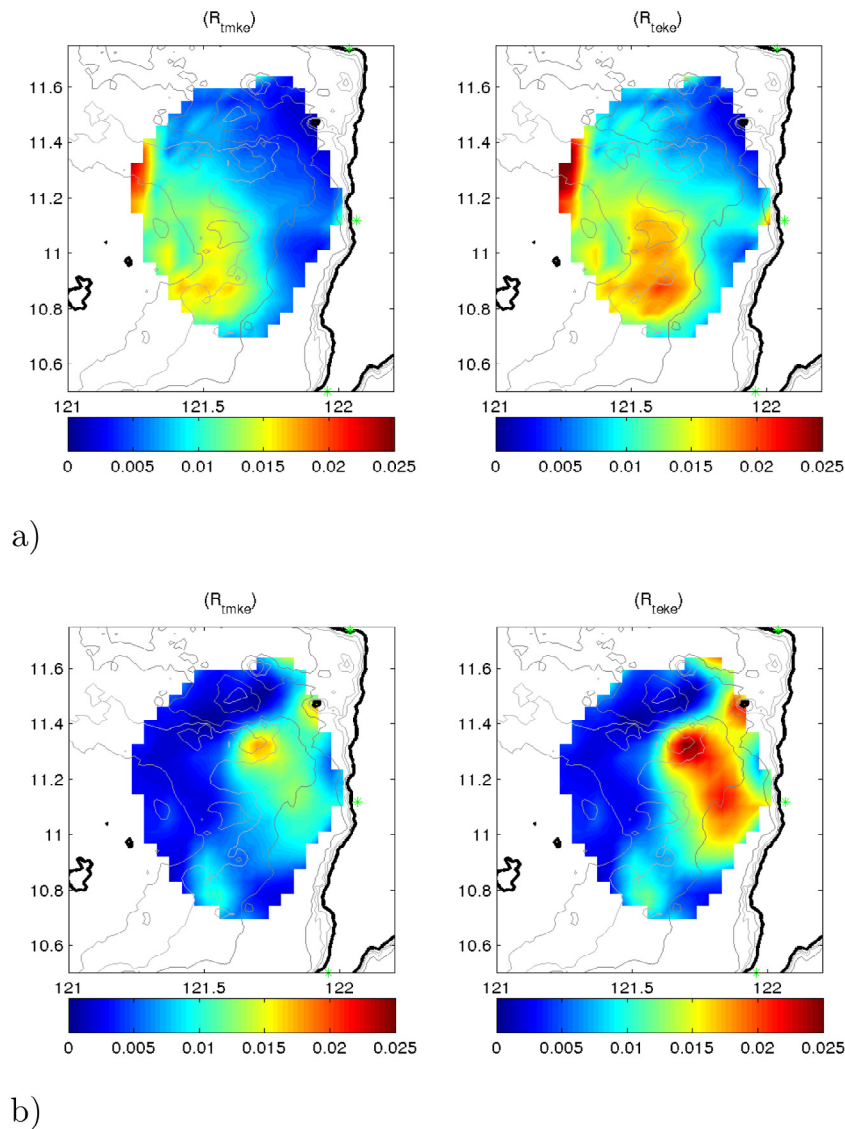
Fig. 6. Contribution of diurnal tidal currents, (a) O_1 and (b) M_2 to the total mean kinetic energy, R_{tmke} and the eddy kinetic energy, R_{teke} averaged for over a year.

To determine the relative contribution of the tidal currents to the mean KE and mean EKE, R_{tmke} and R_{teke} were calculated and shown in Fig. 5b. The tidal currents, u_p and v_p were formed from the four major tidal current constituents analyzed. The distributions of O_1 and M_2 constituents, which contribute much to the tidal KE, are shown in Fig. 6a and b.

The contributions of the tidal currents to both the mean KE and the mean EKE show similar patterns though their contribution to the mean EKE are relatively large ($R_{tmke} = 0.043$ and $R_{teke} = 0.0510$). The regions with highest contributions are on the shallow areas of the Cuyo shelf where there are sharp bends in the 100 m isobath and over which the persistent northward PC jet exists. This suggests the influence of tidal currents on the PC jet, as it accelerates over the shallow part of the shelf. Another high contribution is on the west end of the radar domain, where a strong return flow indicating the Panay Eddy approaches the 100 m isobath of the shallow Cuyo shelf.

From the 4 major constituents, O_1 and M_2 contribute the highest to the mean tidal kinetic energy where O_1 dominates over the shallow shelf while M_2 over the deep channel with sharp bends observed in the 100 m isobath and over which PC jet intensifies as it approach the narrowest constriction of the strait.

3.3. Vertical structure of the tidal component inferred from ADCP

For the mooring located near the relatively narrow part of Panay Strait, tidal variability makes up a large part of the velocity signal. The vertically-averaged frequency spectrum of the ADCP is very similar to the spectrum of the HFDR for periods shorter than 5 days showing strong peaks at K_1, O_1, M_2, and S_2 tidal components (Fig. 7a). The O_1 and M_2 constituents dominate the diurnal and semi-diurnal bands, respectively. Strong energy in the inertial band is absent in the spectrum, presumably because the data in the upper profile (top 50 m) are missing. This suggests the importance of the local wind in generating the peaks in the near-inertial motions from HFDR-derived surface current spectrum.

The large percentage of variance explained by the 4 major tidal constituents (K_1, O_1, M_2, and S_2) are in two distinct layers, centered at 110 m and 470 m for both across and along-channel tidal current components (Fig. 7b). The highest variance at 110 m (11.32%) accounts for the along-channel tidal currents which corresponds to the strong shear where upper layer flows northward into the SCS while strong southward flow below toward the SS during the NEM suggesting a monsoonal relationship (Sprintall et al., 2012). The M_2 constituents mainly contribute to the
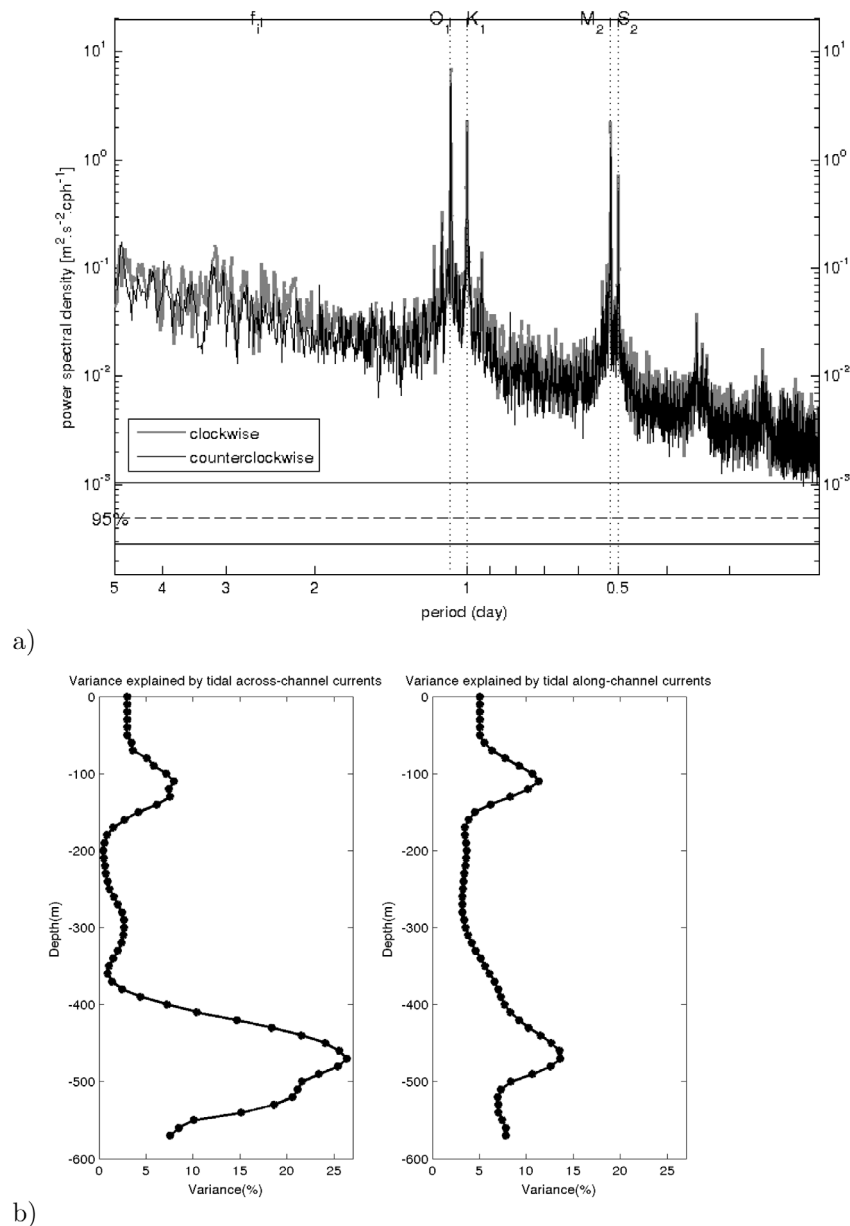
Fig. 7. (a) Rotary power spectra of vertically averaged currents from ADCP. Major tidal constituents and inertial frequency, f_i are indicated on the top x-axis, indicated by vertical dotted lines. (b) Variance explained by 4 major (K_1, O_1, M_2, and S_2) constituents (left) across and (right) along channel.

variance. At 470 m, across-channel tidal currents account for the highest variance (26.33%) which corresponds with the intense thermocline near-inertial motions suggested to be due to Parametric Subharmonic Instability (PSI) of the diurnal internal tide found near 400 m at northern Mindoro Strait in the SCS, which undergoes similar or higher levels of near-bottom mixing than the Panay Sill (Chinn et al., 2012). Chinn et al. (2012) note that PSI of the internal tide can only occur equatorward of the critical latitude where half the tidal frequency is greater than the local inertial frequency (e.g., 14.52° N for K_1 and 13.44° N for O_1). Recent observational work under PhilEx program however, has shown convincing evidence that near the critical latitudes the rates of PSI are vastly enhanced and may be a dominant part of the redistribution of energy throughout the internal wave spectrum (Chinn et al., 2012). The main evidence for PSI was the fortnightly modulation of the near-inertial band, indicating a signal that is often comprised of both upward and downward propagating waves seen near 400 m (Chinn et al., 2012). The

specifics of the physical forcing that allow it to occur at this particular depth however, are uncertain and more work is needed to fully understand the dynamics at work in Mindoro–Panay Strait. The variance explained by mean tidal across-channel currents is attributed mostly to diurnal tide (O_1) over the Cuyo shelf to the west.

The vertical mean KE, EKE and tidal KE are shown in Fig. 8b. In contrast to the mean KE from the surface current, the mean EKE and the mean tidal KE are relatively small, an order of magnitude less and two orders of magnitude less, respectively than the mean KE. The mean KE is highest at 520-m depth which corresponds with the hydraulically controlled benthic overflow in the SCS that acts to ventilate the SS with little seasonal variance (Tessler et al., 2010). Both the highest mean EKE and mean tidal KE are at 470 m depth where a PSI-generated near-inertial wave signal was found by Chinn et al. (2012).

The vertical distributions of R_{tmke} and R_{teke} are shown in Fig. 8b with a peak at 110 m, and two distinct peaks at 110 m and 470
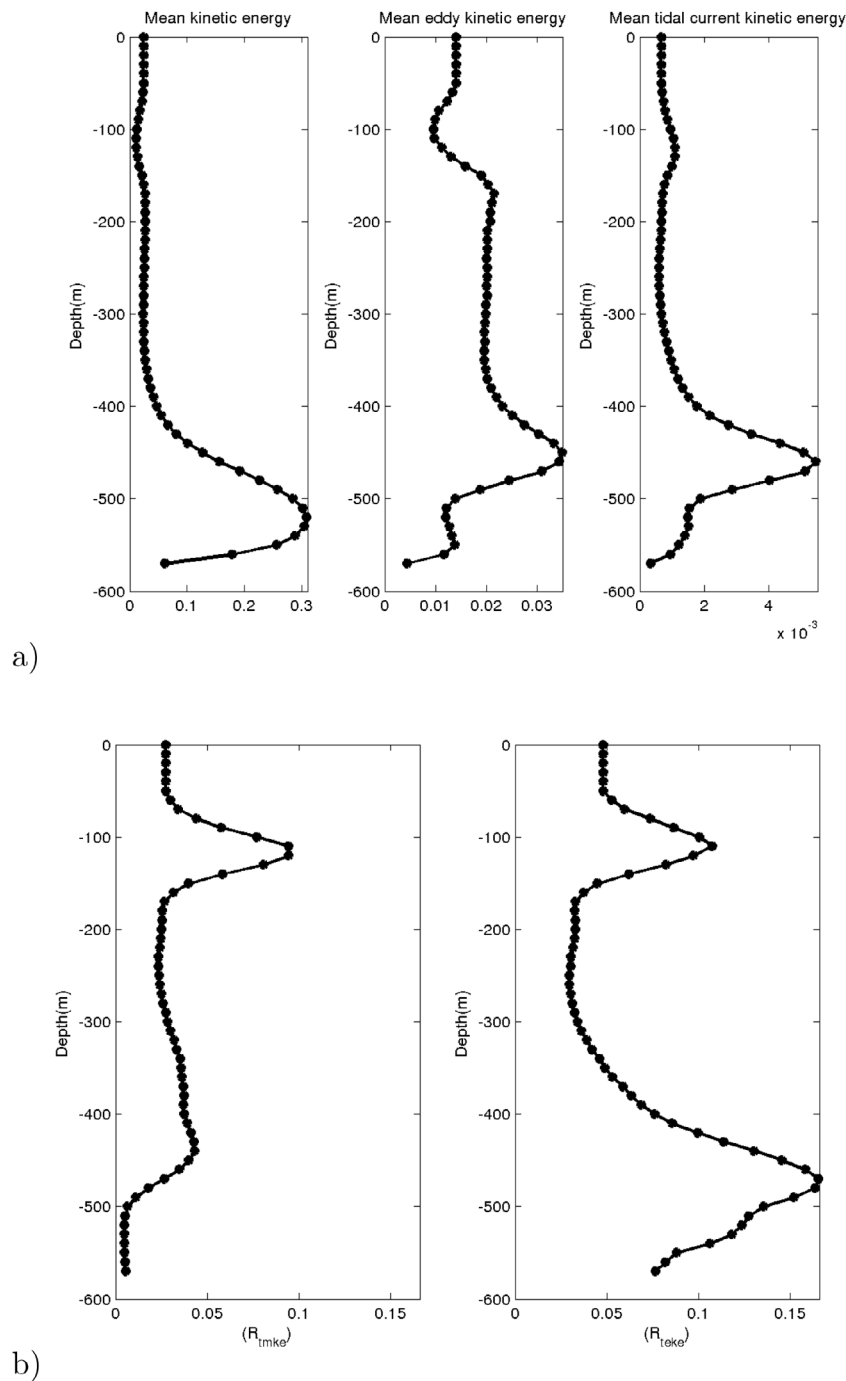
Fig. 8. (a) (left) Mean kinetic energy (KE), (middle) eddy kinetic energy (EKE), and (right) tidal kinetic energy (KE). (b) Contribution of tidal currents to the (left) mean kinetic energy, R_{tmke} and the (right) eddy kinetic energy, R_{teke}.

m, respectively, indicating the dominant tidal activities at shear depth (110 m) during NEM and confirming the PSI-generated thermocline near-inertial motions at 470 m depth discussed above.

3.4. Coherent tides

Harmonic analyses of surface and sub-surface current components (zonal and meridional) were performed using T-tide Matlab package (Pawlowicz et al., 2002). Only the 4 major (K_1, O_1, M_2,

and S_2) tidal constituents inferred from sea level were least-square fitted to the observations, along with a constant and a linear trend.

Maps of the observed tidal current ellipses, major axis amplitudes and phases of the four major constituents (K_1, O_1, M_2, and S_2) are shown in Fig. 9. Tidal ellipses are a compact method used to describe tidal current variance using major and minor axes, inclination and phase. The axes describe the magnitude of the current in 2 orthogonal directions, inclination provides
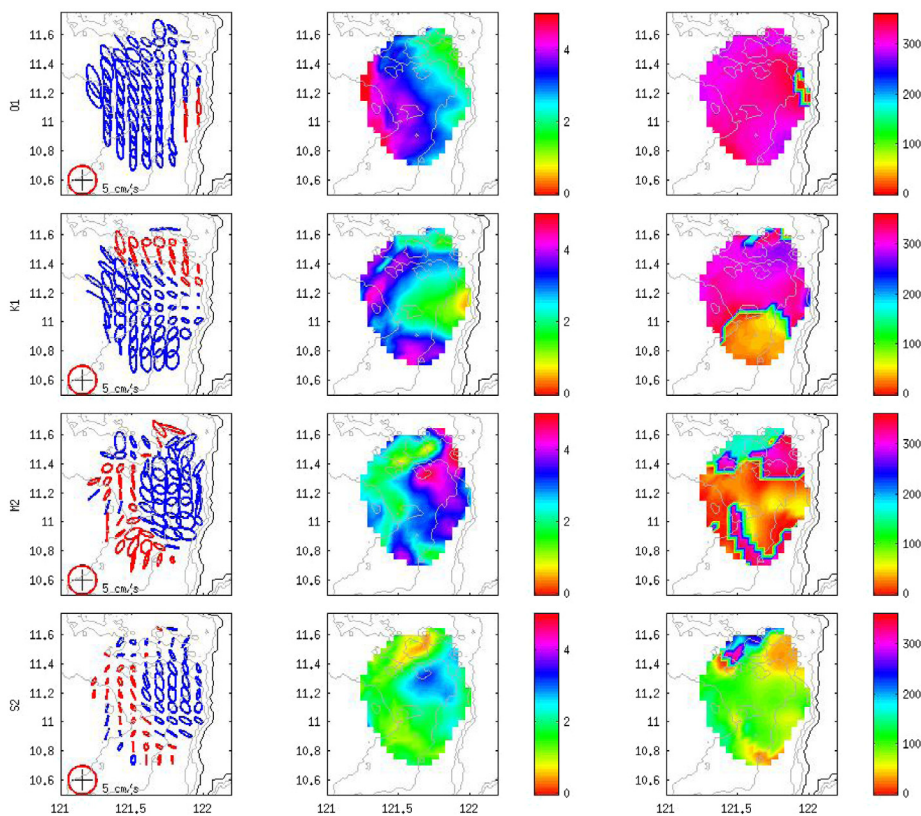
Fig. 9. (Top to bottom) O_1, K_1, M_2, and S_2 (bottom) (left column) ellipses, (middle column) major axis amplitude [cm/s], and (right column) Greenwich phase of HFDR tidal current. Counterclockwise and clockwise ellipses are plotted in red and blue respectively. The phase is defined as the lag of the maximum current (along the northern semi-major axis) with respect to the astronomical phase of M_2 at $0°E$. (For interpretation of the references to color in this figure legend, the reader is referred to the web version of this article.)
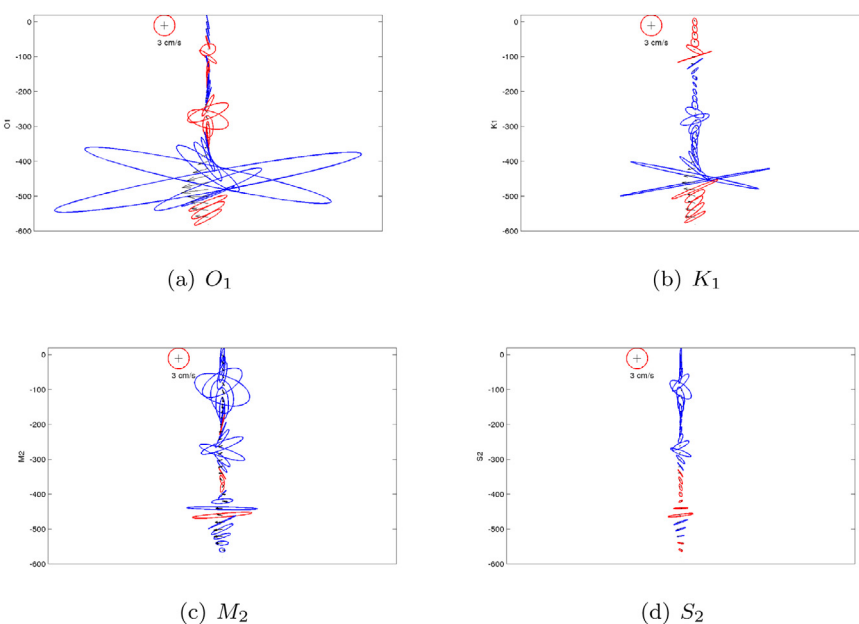
Fig. 10. Averaged ellipses with depth for major tidal constituents. Counterclockwise and clockwise ellipses are plotted in red and blue, respectively. (For interpretation of the references to color in this figure legend, the reader is referred to the web version of this article.)

orientation for the axes and phase indicates time lag from Greenwich when the time vector passes the northern semi-major axis. Diurnal peaks are more pronounced over the shelf with amplitudes increasing to the shallow area. O_1 tidal ellipses are elliptical over the shelf, relatively narrow, and aligned along the channel axes. M_2 has broader and more circular tidal ellipses near the channel, indicating that rotation is relatively important and/or due to transverse reflection effects. The M_2 major axis amplitudes increase towards the narrow constricted part of the strait. S_2 has similar patterns to M_2 though substantially weaker. The large phase gradients across the HFDR coverage indicate strong reversing tidal pressure gradients and likely locations of accelerated currents and internal tide generation. This is most obvious at the deep channel near the sill and at the edge of the shallow shelf with shoals and promontories. Tessler et al. (2010) showed evidence of this strong bottom-enhanced overflow current at Panay Sill with strong tidal variability observed during flood tide with velocities over 70 cms^{-1}. The flow appeared to be hydraulically controlled at the sill with strong turbulent mixing. This Panay Sill overflow water ventilates an upper slab of the Sulu Sea between approximately 600 and 1250 dbar with an estimated residence time of 11 years.

The vertical structure of the tidal ellipses of 4 major tidal constituents (O_1, K_1, M_2 and S_2) remarkably exhibit two sharp peaks consistent with the location of highest variance explained by the tides at 110 m and 470 m, suggesting contributions from baroclinic tidal current Fig. 10. The coherent portion of the semi-diurnal tide (M_2) dominates at 110 m while the coherent diurnal tide (O_1) dominates at 470 m, consistent with the PSI of the diurnal internal tide found at this depth (Chinn et al., 2012).

3.5. Ratio of incoherent to coherent energy

The ratio of incoherent to coherent diurnal and semidiurnal tides in HFDR-derived surface currents are shown in Fig. 11a and b, respectively.

The diurnal frequency band was defined as:

$[O_1 + 1/T >$ diurnal $> K_1 - 1/T]$

and the semi-diurnal frequency band as:

$[M_2 + 1/T >$ semi-diurnal $> S_2 - 1/T]$

where T is the record length.

The K_1 constituent dominated the incoherent tidal band. Incoherent diurnal energy is strong along channel (100 m isobath) over the northern region in between the shoals and down south into the SS (Fig. 11a). The incoherent semi-diurnal energy on the other hand is most significant in the more confined regions than the diurnal, along sharp channel bends (Fig. 11b). A considerable increase of energy westward is evident, particularly in the incoherent diurnal energy. The incoherent portion of the tide is presumably attributable to the surface expression of the internal tide, which seems to be generated near the sill and then topographically steered west over the shallow shelf where incoherent energies are high.

After removing the coherent tidal component as identified by the least squares fit, the diurnal and semi-diurnal tidal bands remained the dominant peaks due to incoherent tidal energy, though K_1 now dominates the diurnal tide band instead of O_1 (Fig. 12a). Chinn et al. (2012) found no evidence to support local or remote forcing mechanism for internal wave generation from their moorings located at both ends of Mindoro–Panay Strait complex. The highly variable internal wave field from HFDR in between those moorings over the Panay Strait, even within the small region covered by HFDR, indicates topographic interactions playing an important role in defining the scales of this variability. Another notable feature in the spectrum is the higher harmonics of diurnal constituents that are still apparent.
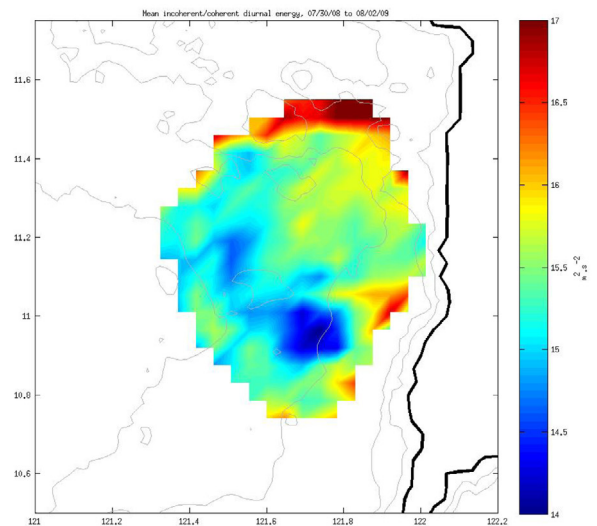
a)
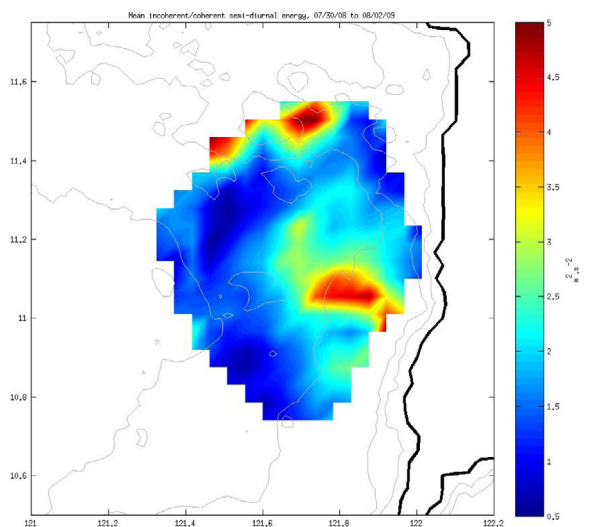
b)

Fig. 11. Ratio of incoherent to coherent (a) diurnal and (b) semidiurnal tides as observed in surface current record.

Vertically over the channel (Fig. 12b), incoherent diurnal energy dominates the upper layer and displays a mode 1, two layer structure with a node at 120 m. The incoherent semi-diurnal energy has more complex modal structure with nodes near the surface and at 240 m.

4. Conclusion

The combination of long duration and high resolution in space, depth and time data from multiple instruments (HFDR, ADCP, and SPG) were used to characterize tides in Panay Strait. The dominant tidal components are K_1, O_1, M_2, and S_2. The barotropic tidal flows in Panay Strait reflect the effect of complex bathymetry as it accelerates through shallow areas and topographic constrictions. Diurnal tides are pronounced over the shallow shelf while semi-diurnal tides are seen in the channel and the shelf break. Vertically, tidal currents are baroclinic. The distributions of incoherent diurnal and semi-diurnal energies vary spatially,
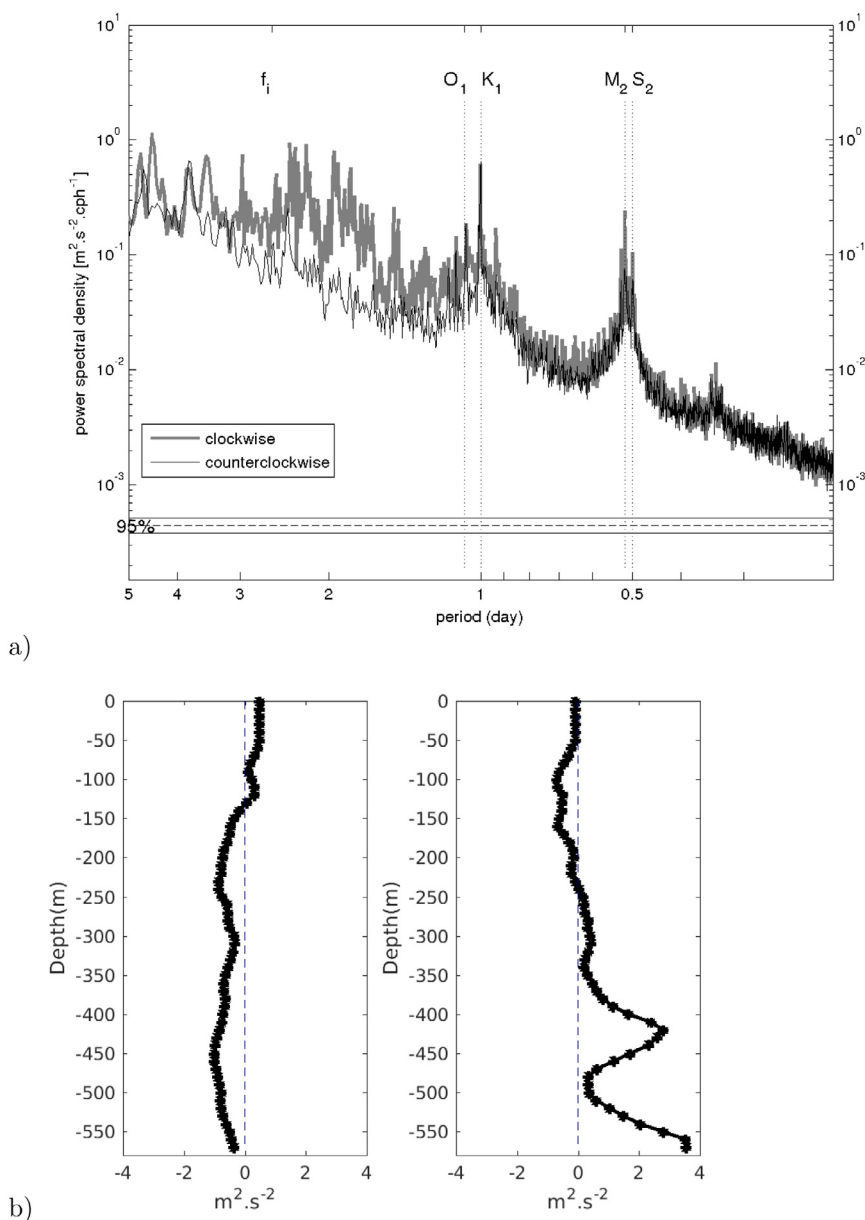
Fig. 12. (a) Rotary power spectra of residual HFDR data over 212 grid points with more than 75% temporal coverage. Major tidal constituents and inertial frequency, f_i are indicated on the top *x*-axis, indicated by vertical dotted lines. (b) Ratio of incoherent to coherent (left) diurnal and (right) semidiurnal tides as observed in the current profile record.

suggesting that topographic interactions may play an important role. Further, Panay Strait is exposed to mesoscale eddies and upwelling. This seasonally varying dynamics may affect the stratification and thus the generation and propagation of internal tides in this area.

CRediT authorship contribution statement

Xavier Flores-Vidal: Software, Formal analysis, Investigation, Resources, Data curation. **Cedric Chavanne:** Software, Formal analysis, Resources, Data curation. **Cesar L. Villanoy:** Supervision, Investigation, Resources, Data curation, Project administration, Funding acquisition. **Pierre Flament:** Conceptualization, Methodology, Formal analysis, Investigation, Resources, Supervision, Data curation, Project administration, Funding acquisition.

Declaration of competing interest

The authors declare that they have no known competing financial interests or personal relationships that could have appeared to influence the work reported in this paper.

Acknowledgments

References

Amedo-Repollo, C.L., Flores-Vidal, X., Chavanne, C., Villanoy, C.L., Flament, P., 2019. Low-frequency surface currents and generation of an island lee eddy in Panay Island, Philippines. J. Phys. Oceanogr. 49 (3), 765–787.

Apel, J.R., Holbrook, J.R., Liu, A.K., Tsai, J.J., 1985. The sulu sea internal soliton experiment. J. Phys. Oceanogr. 15 (12), 1625–1651.

Chavanne, C., Janeković, I., Flament, P., Poulain, P.-M., Kuzmić, M., Gurgel, K.-W., 2007. Tidal currents in the northwestern adriatic: High-frequency radio observations and numerical model predictions. J. Geophys. Res. Oceans (1978–2012) 112 (C3).

Chinn, B.S., Girton, J.B., Alford, M.H., 2012. Observations of internal waves and parametric subharmonic instability in the Philippines archipelago. J. Geophys. Res. Oceans (1978–2012) 117 (C5).

Emery, W., Thomson, R., 2004. Data analysis methods in physical oceanography elsevier. Amsterdam 638pp.

Giese, G.S., Chapman, D.C., Collins, M.G., Encarnacion, R., Jacinto, G., 1998. The coupling between harbor seiches at palawan island and sulu sea internal solitons. J. Phys. Oceanogr. 28 (12), 2418–2426.

Girton, J.B., Chinn, B.S., Alford, M.H., 2011. Internal wave climates of the philippine seas. Oceanography.

Gonella, J., 1972. A rotary-component method for analysing meteorological and oceanographic vector time series. In: Deep Sea Research and Oceanographic Abstracts, Vol. 19 (12). Elsevier, pp. 833–846.

Gordon, A.L., Villanoy, C.L., 2011. The oceanography of the philippine archipelago. Oceanography 13.

Han, W., Moore, A.M., Levin, J., Zhang, B., Arango, H.G., Curchitser, E., Di Lorenzo, E., Gordon, A.L., Lin, J., 2009. Seasonal surface ocean circulation and dynamics in the philippine archipelago region during 2004–2008. Dyn. Atmos. Oceans 47 (1), 114–137.

Hurlburt, H.E., Metzger, E.J., Sprintall, J., Riedlinger, S.N., Arnone, R.A., Shinoda, T., Xu, X., 2011. Circulation in the philippine archipelago simulated by 1/12 degrees and 1/25 degrees global hycom and eas ncom. Oceanography.

Jackson, C.R., Arvelyna, Y., Asanuma, I., 2011. High-frequency nonlinear internal waves around the Philippines. Oceanography.

Jackson, C.R., Da Silva, J.C., Jeans, G., 2012. The generation of nonlinear internal waves. Oceanography 25 (2), 108–123.

Jing, Z., Qi, Y., Du, Y., 2012. Persistent upwelling and front over the sulu ridge and their variations. J. Geophys. Res.: Oceans 117 (C11).

Lermusiaux, P.F., HaLey Jr, P.J., Leslie, W.G., Agarwal, A., Logutov, O.G., Burton, L.J., 2011. Multiscale physical and biological dynamics in the philippine archipelago: predictions and processes. Oceanography 24 (1), 70–89.

Liu, A.K., Holbrook, J.R., Apel, J.R., 1985. Nonlinear internal wave evolution in the sulu sea. J. Phys. Oceanogr. 15 (12), 1613–1624.

May, P.W., Doyle, J.D., Pullen, J.D., David, L.T., 2011. Two-Way Coupled Atmospher-Ocean Modeling Of The PhilEx Intensive Observational Periods. Tech. rep., DTIC Document.

McClean, J.L., Ivanova, D.P., Sprintall, J., 2005. Remote origins of interannual variability in the Indonesian throughflow region from data and a global parallel ocean program simulation. J. Geophys. Res. Oceans 110 (C10).

Pawlowicz, R., Beardsley, B., Lentz, S., 2002. Classical tidal harmonic analysis including error estimates in matlab using t_Tide. Comput. Geosci. 28 (8), 929–937.

Press, W.H., Teukolsky, S.A., Vetterling, W.T., Flannery, B.P., 1996. Numerical recipes in C, Vol. 2. Cambridge university press Cambridge.

Pullen, J., Doyle, J.D., May, P., Chavanne, C., Flament, P., Arnone, R.A., 2008. Monsoon surges trigger oceanic eddy formation and propagation in the lee of the philippine islands. Geophys. Res. Lett. 35 (7).

Sprintall, J., Gordon, A.L., Flament, P., Villanoy, C.L., 2012. Observations of exchange between the south China sea and the sulu sea. J. Geophys. Res. Oceans (1978–2012) 117 (C5).

Storlazzi, C.D., Cheriton, O.M., Van Hooidonk, R., Zhao, Z., Brainard, R., 2020. Internal tides can provide thermal refugia that will buffer some coral reefs from future global warming. Sci. Rep. 10 (1), 1–9.

Tessler, Z.D., Gordon, A.L., Jackson, C.R., 2012. Early stage soliton observations in the sulu sea. J. Phys. Oceanogr. 42 (8), 1327–1336.

Tessler, Z.D., Gordon, A.L., Pratt, L.J., Sprintall, J., 2010. Transport and dynamics of the panay sill overflow in the philippine seas*. J. Phys. Oceanogr. 40 (12), 2679–2695.

White, W.B., Tourre, Y.M., Barlow, M., Dettinger, M., 2003. A delayed action oscillator shared by biennial, interannual, and decadal signals in the Pacific basin. J. Geophys. Res. Oceans 108 (C3).

Zeng, K., Alpers, W., 2004. Generation of internal solitary waves in the sulu sea and their refraction by bottom topography studied by ers sar imagery and a numerical model. Int. J. Remote Sens. 25 (7–8), 1277–1281.

Zhang, X., Li, X., Zhang, T., 2020. Characteristics and generations of internal wave in the sulu sea inferred from optical satellite images. J. Oceanol. Limnol. 38 (5), 1435–1444.